FWI – Full Waveform Inversion

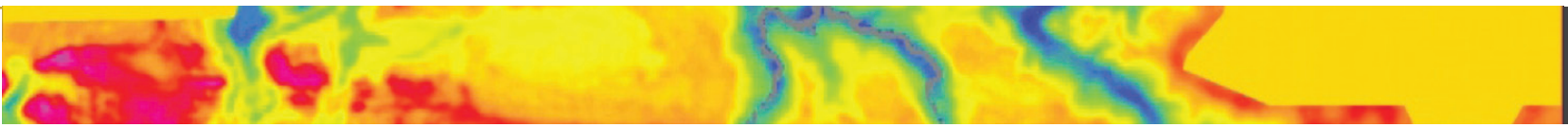

GeoTomo leads the way in near-surface statics and imaging technologies

TomoPlus is the only commercial near-surface software package that offers a Full Waveform Tomography solution for solving complex near-surface statics and velocity problems in areas where karst, low velocity layers, outcropping refractors, and strong velocity contrasts exist. Other near-surface solutions such as Delay-Time, GLI and Traveltime techniques may fail in these complex environments.

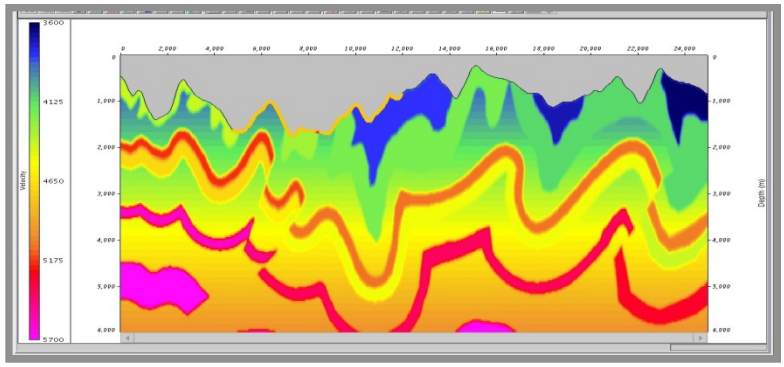

True Model

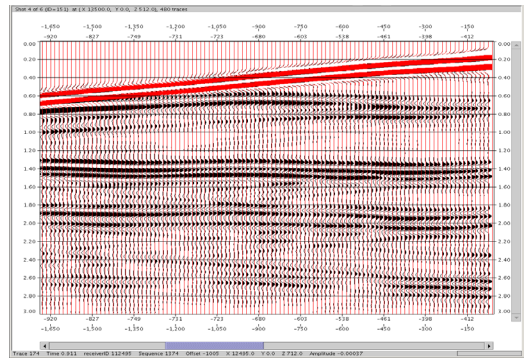

Initial Waveform Comparison

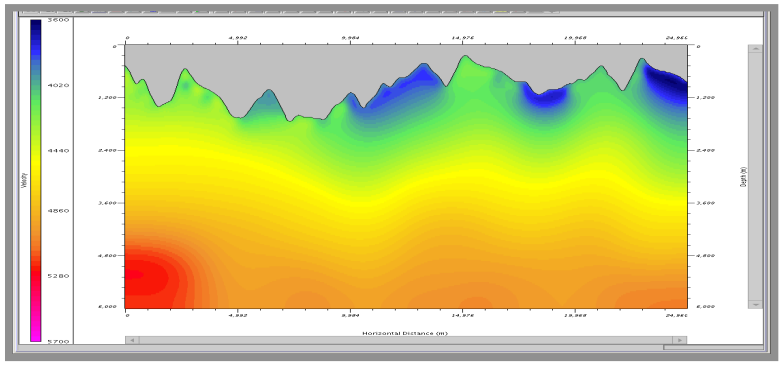

Initial Model

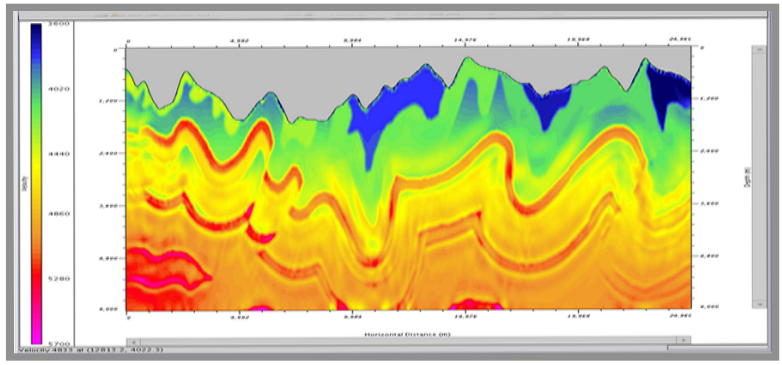

Final FWI Model

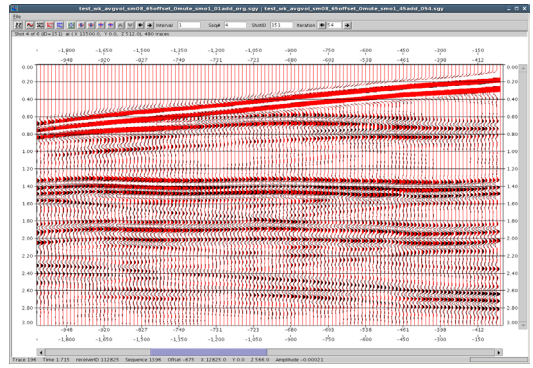

Final Waveform Comparison

Solution Comparison on Complex Foothills Model

True Foothills Model

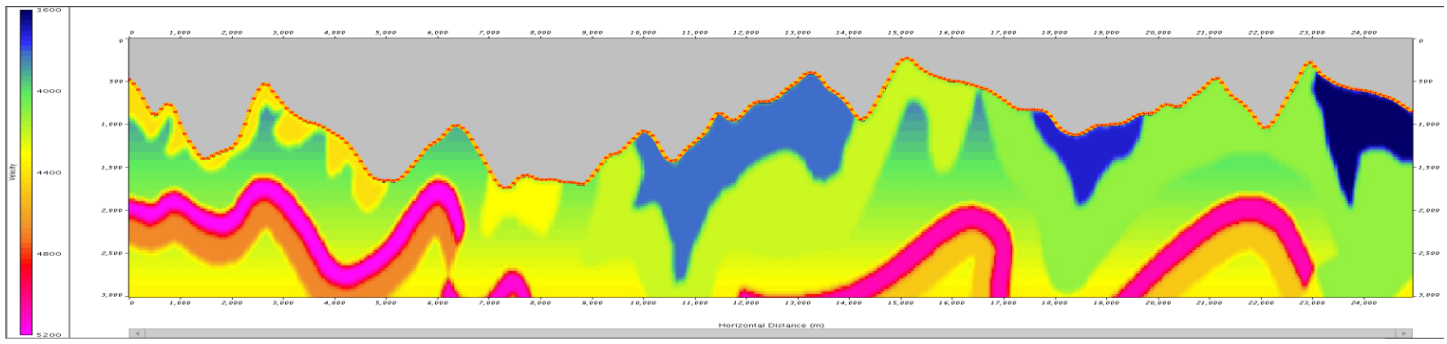

Delay Time Solution

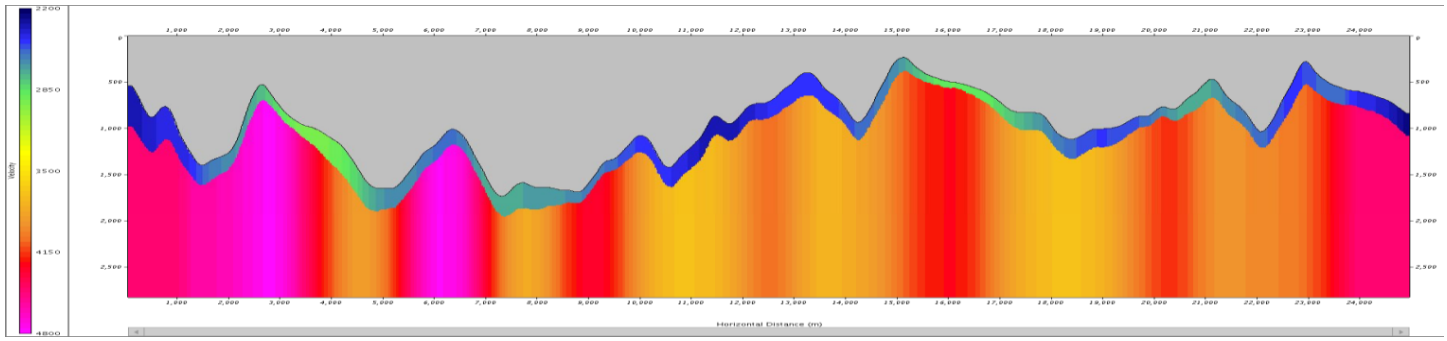

Traveltime Tomography Solution

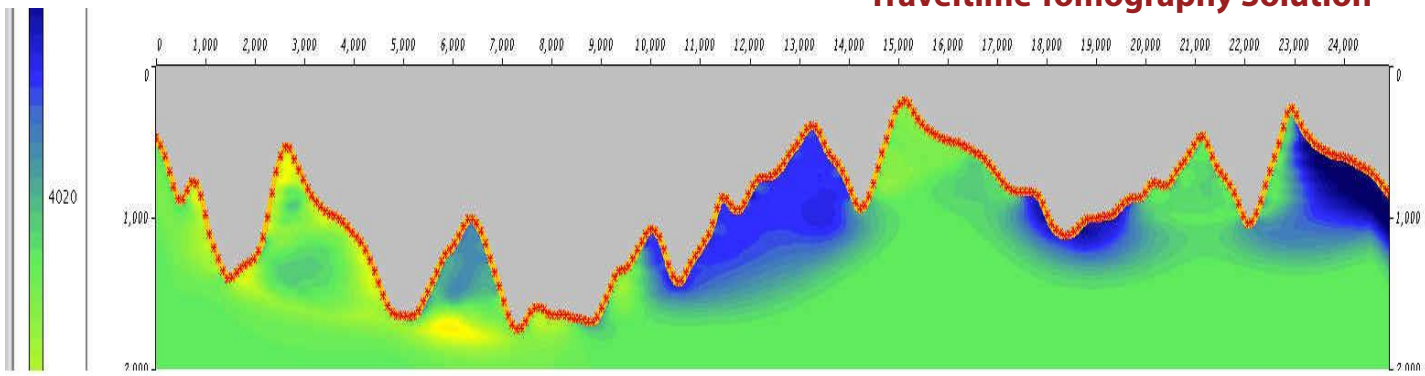

Full Waveform Solution

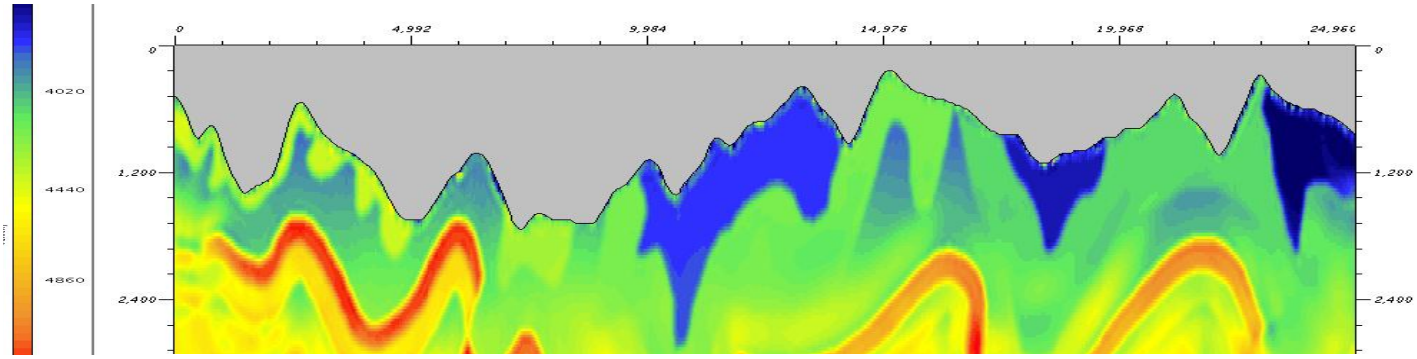

FWI – Full Waveform Inversion

GeoTomo's FWI solution is designed for land, marine and OBC data.

FWI & Traveltime 2D Land Example:

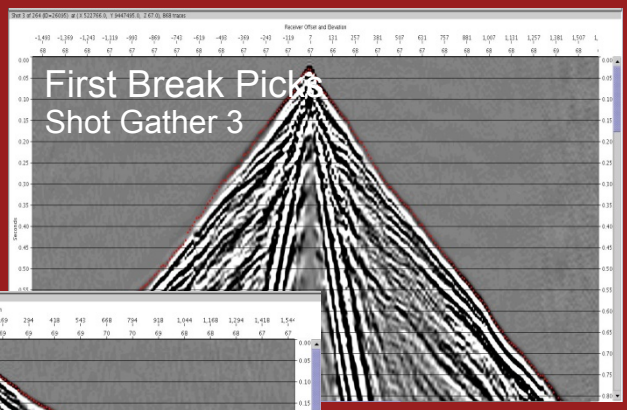

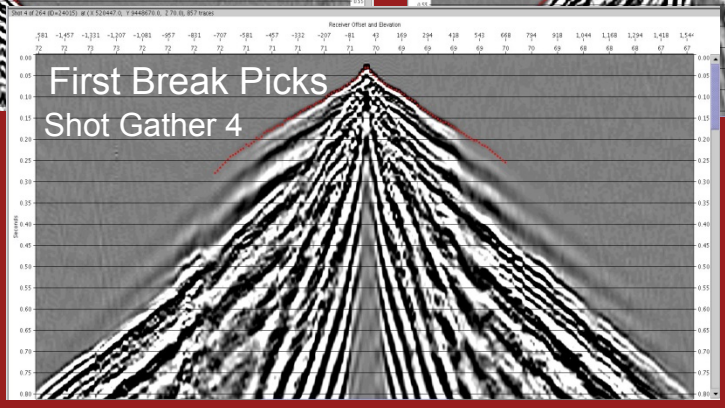

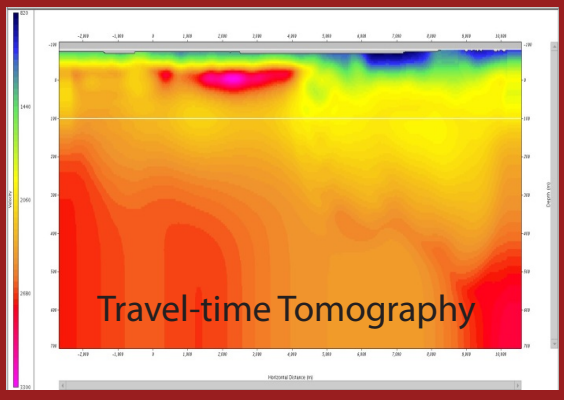

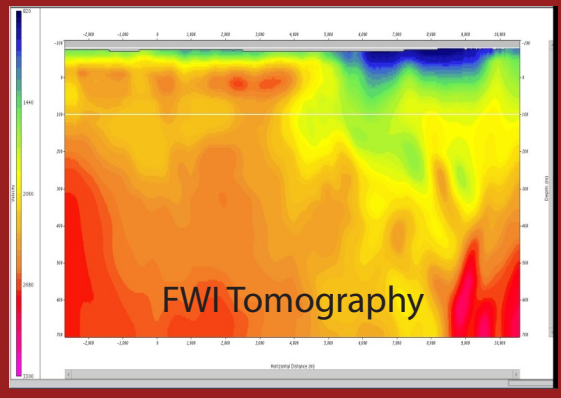

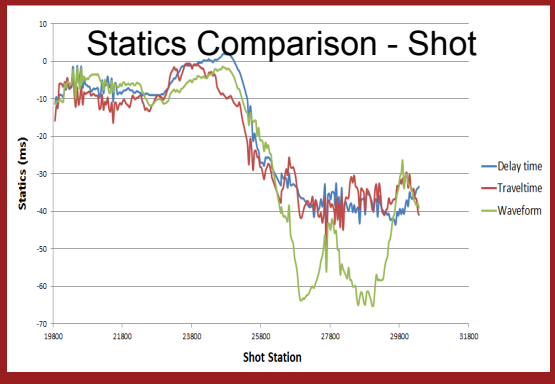

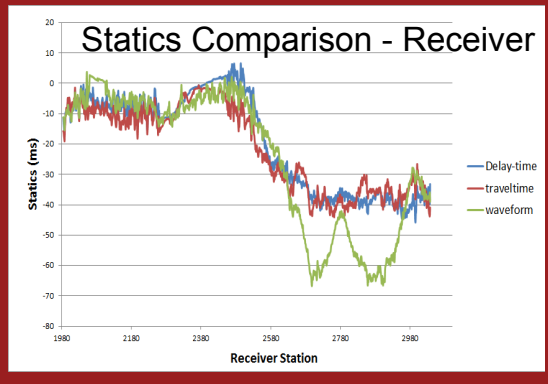

3D acoustic waveform inversion of land data: a case study from Saudi Arabia

Joseph McNeely, Timothy Keho, Thierry Tonellot, Robert Ley, Saudi Aramco, Dhahran, and Jing Chen, GeoTomo, Houston*

Summary

We present an application of time domain early arrival acoustic waveform inversion to 3D seismic land data in Saudi Arabia for the purpose of constructing a near-surface velocity model. Traditional traveltime methods for velocity estimation can be inadequate in arid environments where karst, low velocity layers, outcropping refractors, and strong velocity contrasts are common. We compare near-surface velocity models derived from 3D traveltime tomography and 3D waveform inversion.

Introduction

Successful seismic imaging of low relief structures and stratigraphic traps in arid land environments strongly depends on how accurately the first five hundred meters of the subsurface are known. Surface karst and paleokarst features create a complex near-surface with sinkholes and partially dissolved or collapsed layers. Interbedded limestones and evaporites, often localized, create strong velocity inversions. These features have a complicating and often degrading effect on signal penetration, seismic waves, trace amplitudes, and near-surface velocities. Figure 1 shows the potential effect of these features on seismic data.

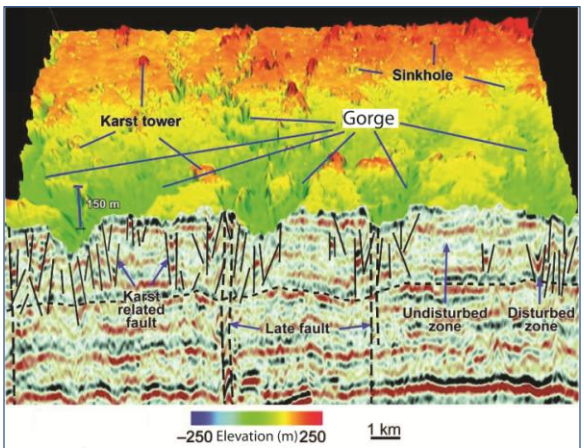

Figure 1. A diagram showing the effect of karst and paleokarst features on seismic data (After Zeng et al, 2011).

This complexity in the near-surface is commonly addressed with standard tools such as single-layer and multi-layer velocity models, refraction statics, and tomographic statics methods (Bridle et al., 2006).

With a more accurate representation of wave propagation physics, waveform inversion has the potential to deliver higher resolution velocity models compared with models obtained by traveltime-based technologies (Virieux and Operto, 2009). Many publications have demonstrated this potential on synthetic or marine data (Sirgue et al., 2009, Vigh et al., 2009). Few applications of waveform inversion to land data have been published, primarily due to poor data quality, and those are mostly restricted to 2D data with very large offsets (Malinowski et al., 2011, Jaiswal et al., 2009).

In this paper we present the first application of waveform inversion to 3D seismic land data in Saudi Arabia. The technique we use is a time domain early arrival acoustic finite difference method. The methodology adopted for this application required first to precondition the data to remove surface waves. Secondly, to reduce the sensitivity of the inversion results to non-acoustic amplitudes, trace scaling was applied to the preconditioned data to favor phase fitting rather than amplitude fitting.

Data preconditioning

A portion of a 3D survey in Saudi Arabia was selected for evaluating waveform inversion. The 42 km^2 test area included 5623 vibrator source points with 4032 channels per source. The maximum offset per source was 4305 m, and source and receiver intervals were both equal to 30 m. The linear sweep frequency was 4 to 92 Hz.

Initial tests of waveform inversion using raw shot data indicated that some data preconditioning was necessary to stabilize the inversion process. The two critical issues were the presence of strong surface wave noise and extreme amplitude variation both within and across source records (Figure 2).

High energy noise and linear noise were addressed by applying a 3D FKxKy filter in the cross-spread domain. Spatially varying amplitudes were adjusted using a three stage process. Amplitude statistics were first computed over a user designed window and stored in the project database. These values were then decomposed surface consistently into source, receiver, and offset terms. Only the source and receiver terms were applied. As a final pre-processing step surface consistent spiking deconvolution was applied in the source and receiver domains. Figure 3 shows a source record after pre-processing.

DOI http://dx.doi.org/10.1190/segam2012-0150.1

The source gathers were then prepared for input into waveform inversion. This involved selection of an appropriate offset range, windowing of the early arrivals, and restricting the frequency range. An offset range of 350 to 2000 m was selected after several trials of forward modeling. Windowing of the early arrivals was achieved by applying top and bottom mutes computed by using the first arrival pick times as a guide, which resulted in a data window of 300 ms. A bandpass filter of 8 to 15 Hz. was applied after examination of frequency/amplitude spectra. Figure 4 shows the prepared early arrivals for one source location.

Time domain early arrival acoustic waveform inversion

The waveform inversion approach adopted in this paper is based on the time domain staggered-grid finite difference acoustic modeling with topography described in Zhang and Zhang (2011). The inversion is achieved by minimizing an L_2 norm in the data space, measuring the misfit between the modeled and observed data with a conjugate gradient algorithm.

An initial velocity model was built by 3D first arrival travel time tomography (Zhang and Toksoz, 1998). This 3D velocity model fits the observed times with an RMS residual of 20 ms. Figure 5 shows the synthetic generated from the initial model for the shot shown in Figure 4. A 9 Hz Ricker source wavelet was used for synthetic generation.

The amplitude variations with offset observed in the field data were very different to the ones observed in the synthetic data. These differences, which can be attributed to attenuation and/or differences in radiation patterns between the field data and the acoustic approximation used to generate the synthetic data, are addressed using an approach inspired by the ones described in Brenders and Pratt (2007) and Shen (2010). We chose to scale the amplitudes of the preconditioned field data to match the offset dependent RMS amplitude variation of the synthetic data produced by the initial model. New scaling was applied to the field data after every fourth iteration to match the offset dependent RMS amplitude variation of the synthetic data computed from the current model. The descent direction used by the conjugate gradient was reset to the gradient direction. This scaling strategy preferentially favors phase fitting during the inversion and de-emphasizes amplitude. Applications on synthetic examples have demonstrated that this strategy helps in the presence of realistic surface consistent amplitude variations (Keho et al., 2012, personal communication).

The 3D velocity model estimated after 20 waveform inversion iterations and a maximum frequency of 15 Hz. is shown in Figure 6. Comparisons of the travel time tomography model with the waveform tomography model reveal several significant differences. The depth slices in Figure 7 show sharper definition of the sinkholes, with higher velocity contrast, and greater lateral velocity variation in the waveform model compared with the travel time model. The cross-sections in Figure 8 show enhanced definition and vertical extension of the sinkhole. Moreover, a high velocity layer can be seen in the upper part of the waveform model while it is not present in the travel time inversion result. This high velocity layer could not be confirmed by any uphole measurements. This result is nonetheless consistent with results obtained on 2D waveform applications in a different area where similar high velocity layers were also imaged and led to more accurate depth imaging results (Tonellot et al., 2012, personal communication). This suggests that this high velocity layer corresponds to a regional formation.

In the absence of borehole measurements, a good quality control available for full waveform inversion consists in comparing synthetic and observed waveforms and evaluating the improvements brought by the inversion process. Figure 9 displays the modeled and synthetic traces after iteration 0 (initial model) and after iteration 20 (final model). The quality of the initial model was good and thus the synthetic traces in the initial model have a good fit with the observed traces, primarily for the first arrivals. Figure 9b, however, shows clearly that the waveform inversion process improved the overall fit and was also able to fit part of the reflected energy as shown by the arrow. These reflections correspond to the high velocity layer present in the waveform inversion model.

Conclusions

We compare a near-surface model derived from 3D acoustic early arrival waveform inversion to a model derived by 3D traveltime tomography for a 3D seismic land survey in Saudi Arabia. The waveform inversion produces a velocity model which shows greater vertical and lateral resolution of karst features and reveals a high velocity layer not present in the traveltime inversion model.

Further evaluation will compare pre-stack depth migration images based on the near-surface velocity models derived from traveltime tomography and waveform inversion.

Acknowledgments

The authors would like to thank Saudi Aramco for permission to publish this paper, and Ralph Bridle for help with preparing the images.

DOI http://dx.doi.org/10.1190/segam2012-0150.1

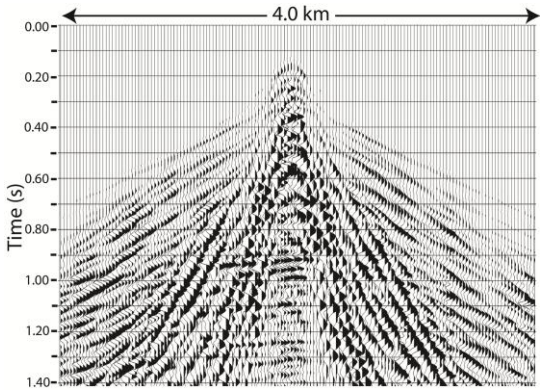

Figure 2. A source gather with time variant gain compensation applied. The strong surface wave noise and spatial amplitude variation are problematic for acoustic modeling.

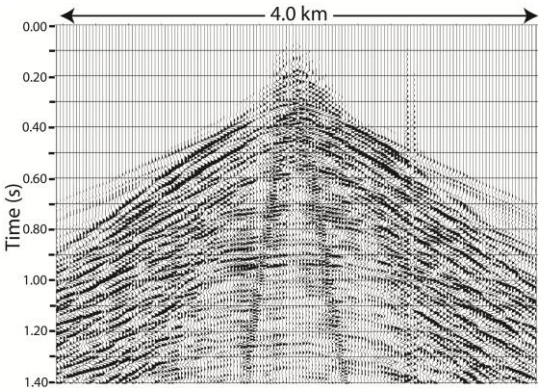

Figure 3. The same source gather shown in Figure 2 after application of 3D FKxKy filter, surface consistent scaling, and surface consistent deconvolution.

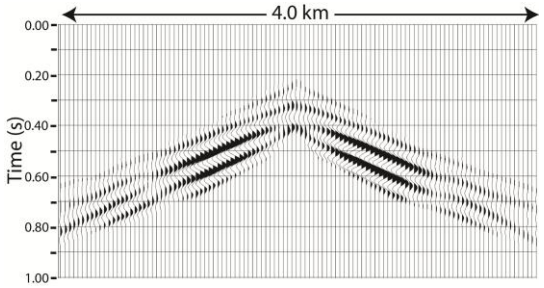

Figure 4. A source gather prepared for input into full waveform inversion. Offsets were limited to 350 to 2000 m, the early arrivals were restricted to a 300 ms window, and an 8-15 Hz. bandpass filter was applied.

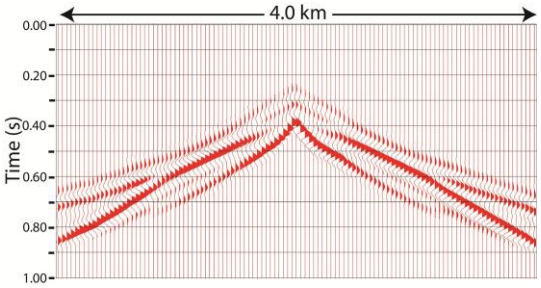

Figure 5. Synthetic traces generated after one pass of forward modeling for the same source location shown in Figure 4. The differences in amplitude justify the use of scaling during the inversion process.

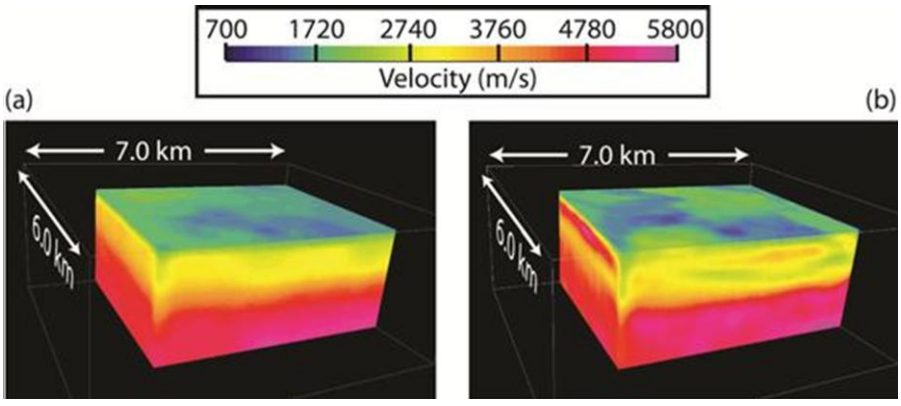

Figure 6. Comparison of oblique views of the 3D traveltime tomography model (a) and the waveform tomography model (b). The elevation scale is the same as in Figure 8.

DOI http://dx.doi.org/10.1190/segam2012-0150.1

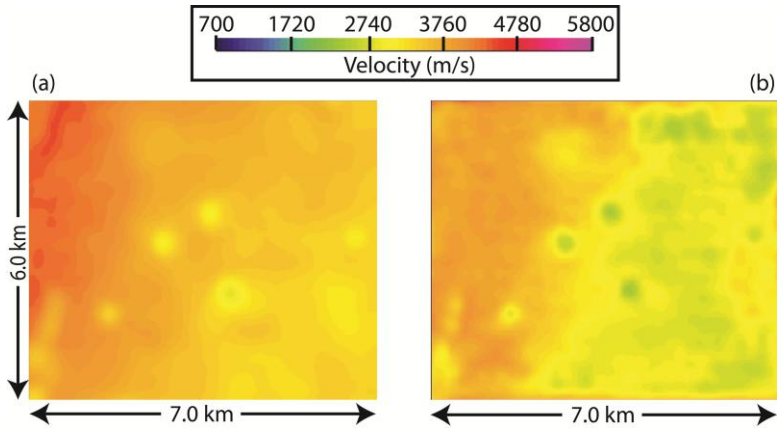

Figure 7. Comparison of depth slices between the travel time tomography model (a) and the waveform tomography model (b). The depth slice shown is 134 m below zero elevation (MSL).

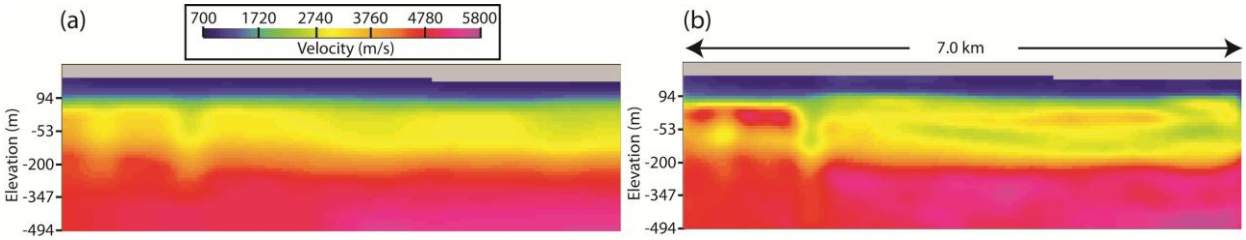

Figure 8. Comparison of cross sections between the traveltime tomography model (a) and the waveform tomography model (b).

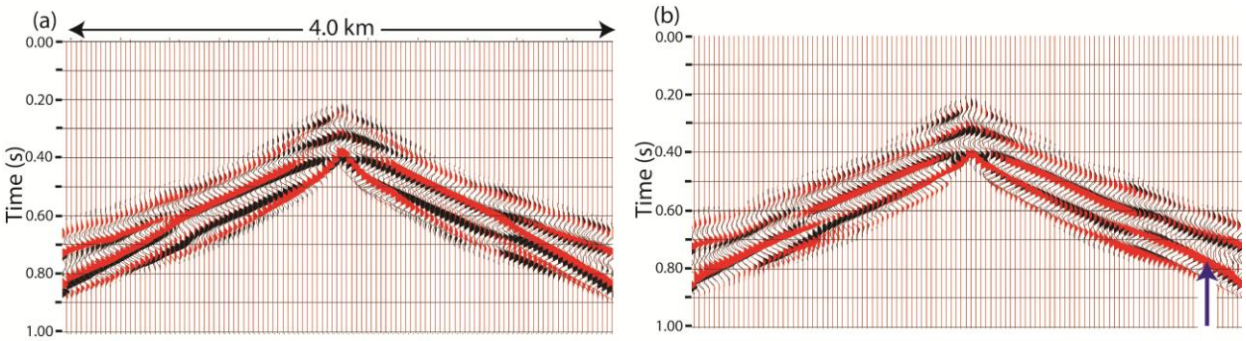

Figure 9. An overlay of the observed (black) and modeled (red) traces. A display of the traces after one pass of forward modeling (a) compared with the traces after 20 iterations (b). The arrow in (b) points to reflected energy which is more accurately modeled after 20 iterations.

DOI http://dx.doi.org/10.1190/segam2012-0150.1

http://dx.doi.org/10.1190/segam2012-0150.1

EDITED REFERENCES

Note: This reference list is a copy-edited version of the reference list submitted by the author. Reference lists for the 2012 SEG Technical Program Expanded Abstracts have been copy edited so that references provided with the online metadata for each paper will achieve a high degree of linking to cited sources that appear on the Web.

REFERENCES

Brenders, A. J., and R. G. Pratt, 2007, Efficient waveform tomography for lithospheric imaging: Implications for realistic 2D acquisition geometries and low frequency data: Geophysical Journal International, **168**, 152–170.

Bridle, R., N. Barsoukov, M. Al-Homaili, R. Ley, and A. Al-Mustafa, 2006, Comparing state-of the art near-surface models of a seismic test line from Saudi Arabia: Geophysical Prospecting, **54**, 667–680.

Jaiswal, P., C. Zelt, R. Dasgupta, and K. Nath, 2009, Seismic imaging of the Naga Thrust using multiscale waveform inversion: Geophysics, **74,** no. 6, WCC129–WCC141.

Malinowski, M., S. Operto, A. Ribodetti, 2011, High-resolution seismic attenuation imaging from wide-aperture onshore data by visco-acoustic frequency-domain full-waveform inversion: Geophysical Journal International, **186**, 1179–1204.

Shen, X., 2010, Near-surface velocity estimation by weighted early-arrival waveform inversion: 80th Annual International Meeting, SEG, Expanded Abstracts, 1975–1979.

Sirgue, L., O. I. Barkved, J. P. Van Gestel, O. J. Askim, and J. H. Kimmedal, 2009, 3D waveform inversion on Valhall wide-azimuth OBC: 71st Conference & Exhibition, EAGE, Extended Abstracts, U038.

Vigh, D., E. W Starr, and J. Kapoor, 2009, Developing earth models with full waveform inversion: The Leading Edge, **28**, 432–435.

Virieux, J., and S. Operto, 2009, An overview of full-waveform inversion in exploration geophysics: Geophysics, **74**, no. 6, WCC1–WCC26.

Zhang, J., and N. Toksoz, 1998, Nonlinear refraction traveltime tomography: Geophysics, **63**, 1726–1737.

Zhang, W., and J. Zhang, 2011, Full waveform tomography with consideration for large topography variations: 81st Annual International Meeting, SEG, Expanded Abstracts, 2539–2542.

Zeng, H., G. Wang, X. Janson, R. Loucks, Y. Xia, L. Xu, and B. Yuan, 2011, Characterizing seismic bright spots in deeply buried, Ordovician paleokarst strata, Central Tabei uplift, Tarim Basin, Western China: Geophysics, **76**, no. 4, B127–B137.